Tampere University

Roosa Mäkitalo

INTERFEROMETRIC AUTOCORRELATION MEASUREMENT OF SUPERCONTINUUM LIGHT BASED ON TWO-PHOTON ABSORPTION

Faculty of Engineering and Natural Sciences
Bachelor of Science Thesis
November 2020

ABSTRACT

Roosa Mäkitalo: Interferometric Autocorrelation measurement of Supercontinuum light based on Two-Photon Absorption
Bachelor of Science Thesis
Tampere University
Science and Engineering
November 2020

Measuring the coherence properties of supercontinuum light is important as many applications require specific coherence characteristics. Studying the coherence of ultrashort light pulses requires special methods, and this thesis presents a cost-effective measurement method that offers direct information on the second-order coherence properties of ultrashort supercontinuum pulses.

This thesis familiarizes the reader with supercontinuum generation and two-photon absorption, which is a nonlinear phenomenon used in the experimental part. The basics of autocorrelation measurements are also introduced, as they are a typical way to characterize ultrafast pulses.

The experimental part of the thesis includes measurements of coherent and incoherent supercontinuum light, which is generated using a Ti:Sapphire laser and a photonic crystal fiber. The achieved interferometric autocorrelation results are discussed, and it can be concluded that the measurement method proves to be successful in measuring the second-order coherence properties of supercontinuum light.

Keywords: supercontinuum, coherence, interferometric autocorrelation, two-photon absorption

TIIVISTELMÄ

Roosa Mäkitalo: Superjatkumovalon kaksifotoniabsorptioon perustuva interferometrinen autokorrelaatiomittaus
Kandidaatintyö
Tampereen yliopisto
Teknis-luonnontieteellinen
Marraskuu 2020

Superjatkumovalon koherenssiominaisuuksien mittaaminen on tärkeää, sillä monet superjatkumovalon sovellukset vaativat tiettyjä koherenssipiirteitä. Ultralyhyiden valopulssien koherenssin tutkiminen vaatii erityisiä mittausmenetelmiä. Tässä kandidaatintyössä esitellään kustannustehokas mittausjärjestely, jolla voidaan mitata ultralyhyiden superjatkumopulssien toisen asteen koherenssiominaisuuksia.

Kandidaatintyössä esitellään superjatkumon syntyminen sekä kaksifotoniabsorptioilmiö, jota hyödynnetään työn kokeellisessa osuudessa. Lisäksi työssä käydään läpi autokorrelaatiomittausten perusperiaatteet, sillä ne ovat usein käytetty tapa ultranopeiden pulssien ominaisuuksien selvittämiseen.

Kokeellinen osuus esittelee mittaukset koherentilla ja epäkoherentilla superjatkumovalolla, jotka luodaan titaanisafiirilaserilla ja fotonikidekuidulla. Mittausten tuloksena saadaan kummallekin valotyypille interferometrinen autokorrelaatio. Johtopäätöksenä mittausmenetelmän todetaan mittaavan superjatkumovalon toisen asteen koherenssiominaisuuksia onnistuneesti.

Avainsanat: superjatkumo, koherenssi, interferometrinen autokorrelaatio, kaksifotoniabsorptio

CONTENTS

1 INTRODUCTION

Supercontinuum light is spectrally broad light, which can be generated by injecting high intensity narrowband light into a nonlinear medium. Supercontinuum generation is a complex nonlinear process, first discovered in 1970 using bulk glass [1], and which has since become more widespread with the development of high intensity lasers and highly nonlinear optical. Because of its unique properties as a light source and many potential applications, supercontinuum light has remained an intense subject of research.

Supercontinuum light has characteristics which makes it the ideal light source for multiple applications including, but not limited to, spectroscopy, metrology and communications. Depending on the application, supercontinuum light should meet specific requirements in terms of coherence. Applications in metrology, for example, require supercontinuum light with a long coherence time and high phase stability, while applications in imaging and sensing only require low intensity noise. Supercontinuum light is typically generated using ultrashort laser pulses with duration on the femtosecond-timescale.

Reports of measuring the coherence properties of supercontinuum light utilizing two-photon absorption have been demonstrated [2, 3]. However, in these reports light is characterized using the normalized degree of spectral coherence, which gives only partial information about the coherence of the supercontinuum pulses. The complete description of the coherence can be achieved by measuring the correlations functions of the second-order coherence of nonstationary light [4], and nonlinear autocorrelation measurements such as intensity autocorrelation and interferometric autocorrelation can provide partial information on the second-order degree of coherence of light.

This thesis presents a simple and low-cost method for measuring the interferometric autocorrelation of supercontinuum light. Interferometric autocorrelation measurements are a common way to study the coherence and phase of ultrashort pulses, as well as the duration of the pulses [5]. The measurement method is based on two-photon absorption, which is a nonlinear phenomenon often used in autocorrelation measurements. The results presented in this thesis offer quantitative information on the coherence of the supercontinuum light used as well as some qualitative insight into the presence of coherent sub-structures under the temporal envelope of the supercontinuum light pulses.

This thesis first introduces the theoretical background behind the phenomena that is necessary for understanding the experimental part. Specifically, the basics of supercontinuum generation are explained in chapter 2, and chapter 3 describes two-photon absorp-

tion, on which the measurement method is based. Chapter 4 then presents the concept of autocorrelation measurements. Experiments are reported in chapter 5, going through the experimental laboratory setup used and subsequently presenting and discussing the results of the experiments. Conclusion of the achieved results is given in chapter 6.

2 SUPERCONTINUUM GENERATION

Supercontinuum (SC) generation refers to a nonlinear process that results in significant spectral broadening of an initially narrow-band light. This process is complex and arises from multiple nonlinear effects, depending on the material and laser light used for the generation. A supercontinuum can be generated in different materials, including optical fibers, and bulk glass where it was first demonstrated in 1970 [1]. Nowadays, the most commonly used media are highly nonlinear optical fibers, and in particular photonic crystal fibers with properties that can be tailored for different wavelengths [6].

In addition to the material used, the SC generation process depends on the characteristics of laser light used. Supercontinuum can be generated both with continuous-wave lasers and pulse lasers, but in practice the latter ones are more commonly used as they provide higher peak power and can seed nonlinear effects more efficiently [7]. In the next section we concentrate on supercontinua generated with pulsed laser sources, which is also the type of source that was used in the experimental part to generate a supercontinuum.

2.1 Physical background

In order to understand supercontinuum generation, one must consider the different nonlinear dynamics underlying the process. The SC generation process is nowadays well-known, significantly due to the extensive experimental work and simulations done in the two past decades. The most relevant processes behind supercontinuum generation are discussed briefly in this chapter. The discussion focuses on light propagating in waveguides, such as an optical fiber, as those are typically used for SC generation.

2.1.1 Dispersion

Dispersion denotes the material refractive index dependence on the wavelength of light. Material dispersion arises from the interaction between the electrons in a material and an electromagnetic wave [8]. Its manifestation can be typically observed in with a prism that separates the different colours of white light. This occurs due to material dispersion that causes the different wavelengths to be refracted at different angles in the prism.

When light is guided into a waveguide, such as an optical fiber, another form of dispersion becomes relevant, waveguide dispersion, which is caused by the modes (the electric field distributions) spatial distribution to be wavelength-dependent. Shorter wavelengths tend to be more confined to the core of the optical fiber, and thus experience a higher refractive index than longer wavelengths where modes partially extend to the cladding [7].

Dispersion affects both the phase velocity and the group velocity of an electromagnetic wave. Group velocity dispersion (GVD) causes light pulses containing many frequencies to broaden temporally, as different wavelengths propagate at different velocities. A parameter for describing GVD is β_2, which appears in the Taylor series approximation of the propagation constant $\beta(\omega)$ that describes how different wavelengths (frequencies) propagate in a medium [7].

The sign of the GVD parameter β_2 is particularly relevant for supercontinuum generation. For $\beta_2 > 0$, the electromagnetic wave experiences normal dispersion, whereas $\beta_2 < 0$ refers to the anomalous dispersion regime. When an optical pulse experiences normal dispersion, its high-frequency components propagate slower than its low-frequency components. In the anomalous dispersion regime, the opposite occurs. The wavelength where β_2 changes its sign is called the zero dispersion wavelength (ZDW). For optical fibers, this is a crucial parameter to consider, when designing a setup for supercontinuum generation, because the nonlinear effects that induce the spectral broadening behave differently for normal and anomalous dispersion regimes [7].

2.1.2 Nonlinear processes in fibers

Nonlinear optics refers to the interaction between an optical electric field and a material being nonlinear. This becomes relevant when the optical intensity is high, leading to the electric field amplitude being comparable to the interatomic forces of the material. Thus, the electrons cannot be treated as harmonic oscillators, as their oscillations in response to the electric field become nonlinear [9].

Optical nonlinearity is often described via polarization $\tilde{P}(t)$, which equals the dipole moment per unit volume. The linear model, where electrons are treated as harmonic oscillators, states that the polarization of a material is proportional to on the applied optical field amplitude $\tilde{E}(t)$ as

$$\tilde{P}(t) = \epsilon_0 \chi^{(1)} \tilde{E}(t), \tag{2.1}$$

where ϵ_0 is the vacuum permittivity and $\chi^{(1)}$ is the linear susceptibility. In nonlinear optics, the higher-order terms of polarization must be taken into account. The dependence of polarization on the optical field is then given by:

$$\tilde{P}(t) = \epsilon_0 \left[\chi^{(1)} \tilde{E}(t) + \chi^{(2)} \tilde{E}^2(t) + \chi^{(3)} \tilde{E}^3(t) + ... \right], \tag{2.2}$$

where $\chi^{(2)}$ and $\chi^{(3)}$ are the second- and third-order nonlinear optical susceptibilities,

respectively. In Equations 2.1 and 2.2 $\tilde{P}(t)$ and $\tilde{E}(t)$ are scalar quantities. For vector treatment, the susceptibilities become tensors of rank $n+1$, where n is the order of the susceptibility [9].

The time-varying polarization described in Equation 2.2 is important for nonlinear optical phenomena, because it can give rise to wave components of new frequencies [9]. In some cases, some terms in Equation 2.2 do not need to be considered. For example, in silica fibers the second-order susceptibility term can be neglected due to symmetry in the material. Thus, the light propagating in a silica fiber does not experience the effects of second-order nonlinearity, that gives rise to effects such as e.g. second-harmonic generation and sum-frequency generation. [7]

We next introduce the most important nonlinear processes behind supercontinuum generation in fibers. Supercontinua can be generated with various lasers and fibers, and we restrict ourselves to dynamics which are relevant to the characteristics of the laser and fiber used in our experiments. The descriptions are kept rather short, and for a more in-depth description the reader may refer to [7].

Optical Kerr effect

The Kerr effect (also known as the quadratic electro-optic effect) refers to a phenomenon, where the refractive index of the material changes as an electric field interacts with the material. The change in the refractive index in the Kerr effect is proportional to the square of the electric field. [8]

The Optical Kerr effect refers specifically to the case, where a high-intensity beam propagates through a nonlinear optical medium. The optical Kerr effect reflects the dependence of the refractive index of the material on the intensity of the indicent electric field. The change Δn in the refractive index of the material induced by the intense electric field is given by

$$\Delta n = n_2 I, \tag{2.3}$$

where n_2 is the nonlinear-index coefficient and I is the incident light intensity. The optical Kerr effect follows essentially from the nonlinear polarization of the material [7].

Self Phase Modulation

Self phase modulation (SPM) arises from the intensity-dependent refractive index of a material (optical Kerr effect). As an optical pulse propagates in the material, the time-varying intensity modulates the refractive index, that in turn causes a time-dependent phase change to the propagating optical pulse. This is known as self phase modulation, and it manifests as a chirp in the laser pulse [7]. Chirp means that the frequency of the pulse is time-dependent. For example, in an up-chirped pulse the shorter wavelengths

travel faster than the long ones, and are thus located on the leading edge of the pulse [8].

SPM induces spectral broadening. The strength of the broadening is dependent on the input pulse peak power and the initial chirp of the pulse. For intense, ultrashort pulses or long fibers SPM can broaden the spectrum significantly, making it an important process for supercontinuum generation [7]. Self phase modulation alone does not induce temporal broadening [5].

A phenomenon similar to SPM is cross phase modulation (XPM), where two or more pulses with different wavelengths modulate each other's refractive indices. The spectral broadening due to XPM can be asymmetric, whereas SPM leads to symmetric broadening with respect to the center frequency [7].

Solitons

In the regime of anomalous dispersion, the effects of dispersion and SPM can exactly balance each other. This leads to the generation of optical solitons. A first-order ($N = 1$) soliton is a wave that propagates through a medium preserving its temporal and spectral shape. Solitons with a higher order N change their shape periodically as they propagate [7].

Femtosecond-timescale laser pulses often have a temporal shape of a hyperbolic secant, and thus, they can be modeled as high-order solitons. These high-order solitons are unstable, and they will break-up into fundamental, first-order solitons, a process known as soliton fission. Soliton fission is caused by perturbations such as high-order dispersion or Raman scattering. The center frequencies of the resulting fundamental solitons can then be shifted towards lower frequencies due to Raman scattering [6].

Soliton dynamics is the main cause of spectral broadening toward the longer wavelengths in the regime of anomalous dispersion supercontinuum as is the case in the experimental part of this thesis.

Four-Wave Mixing and Modulation Instability

Four-wave mixing (FWM) is a broadening mechanism that, as the name suggests, involves the interaction of four optical fields with distinct frequencies with a third-order nonlinearity. Most of the combinations of the four fields will not cause FWM as they have a phase mismatch. For a certain frequency to be amplified, it has to fulfill the phase-matching condition, which arises from the conservation of energy and momentum. For a laser pulse with a center frequency ω_0 in the anomalous dispersion, if the phase-matching condition is met, weak sidebands around ω_0 can get symmetrically amplified due to FWM [7].

The phase-matching condition can also be fulfilled in the presence of SPM and XPM.

FWM of this manner is known as modulation instability (MI). MI describes the phenomenon in time-domain, whereas FWM describes it in frequency-domain. For strong electric fields (high intensity laser pulses), MI can amplify noise around the center wavelength, which will result in the loss of coherence [10]. MI is present typically in the regime of anomalous dispersion, where the phase-matching condition is met, but its appearance in the normal dispersion is also possible under suitable circumstances [7].

In SC generation with a duration of few hundred femtoseconds or longer, FWM/MI is a significant cause of spectral broadening. This holds especially for picosecond and nanosecond pulses, for which it is the leading cause of spectral broadening. However, it can also contribute to the spectral broadening of femtosecond-timescale pulses [7].

Stimulated Raman scattering

Raman scattering refers to an inelastic scattering process, where part of the energy of an optical wave propagating in a material is stored to the vibrational states of the molecule of the material. For a high-intensity laser, the interaction between the light and the medium can cause stimulated Raman scattering (SRS), where weak light with wavelength longer (the frequency is smaller) than that of the original wave is amplified. This type of Raman scattering is called Stokes scattering, and it causes a red-shift, i.e. the spectrum is broadened toward longer wavelengths. [7] However, when acting together with FWM, SRS can also broaden the spectrum to shorter wavelengths [11]. In addition, SRS can also amplify noise [7].

For pulse durations shorter than picoseconds, the pulse bandwidth can be broader than the gain spectrum of SRS, which causes a red-shift of the spectrum towards longer wavelengths. In the anomalous dispersion regime, where soliton dynamics apply, this is known as soliton self-frequency shift. If the incident laser pulse can be modelled as a high-order soliton, SRS can disturb the soliton, causing a soliton fission phenomenon discussed previously. The resulting fundamental solitons may then be shifted further towards long wavelengths. SRS and soliton dynamics play a central role in supercontinuum generation in the anomalous dispersion regime, broadening the spectrum significantly towards longer wavelengths [7].

2.2 Photonic Crystal Fiber

A typical optical fiber consists of a core and a cladding surrounding the core. The cladding and the core have different refractive indices such that the light experiences total internal reflection at the core-cladding interface as the light propagates at a suitable angle with respect to the interface in question. In a photonic crystal fiber (PCF), the cladding consists of air holes placed in a lattice arrangement around the core. The core may be either made out of solid glass, or hollow [6]. Figure 2.1 shows the structure of a photonic crystal fiber.

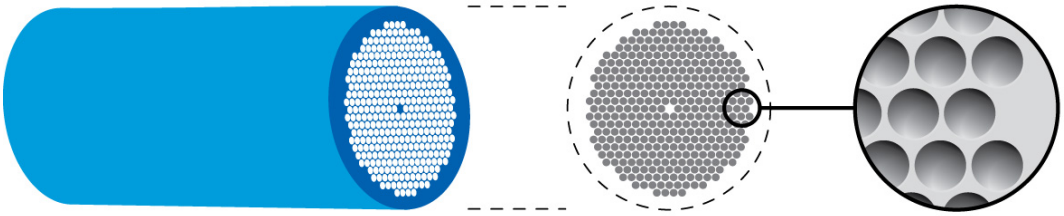

Figure 2.1. *The structure of a photonic crystal fiber: a narrow core is surrounded by a periodic lattice of air holes. [12]*

For conventional single-mode fibers, the difference between the refractive indices of the core and the cladding is rather small. For a photonic crystal fiber, however, the refractive index difference is much larger, affecting the waveguide properties, such as waveguide dispersion being stronger. The structure of a PCF also leads to high nonlinearity, as light is confined to the narrow core [6].

By engineering the hole lattice structure around the core, namely the diameters of the holes and the distance between the holes, the dispersion profile of a PCF can be tailored. For example, the zero dispersion wavelength of the fiber can be shifted to the wavelength range of a certain light source. This has allowed an increasing number of studies on supercontinuum generation for different dispersion regimes and pump wavelengths [6].

2.3 Applications

As the processes behind supercontinuum generation are nowadays well-known, and a large variety of lasers and engineered optical fibers are commercially available, supercontinuum light has become an important light source for many applications. A broadband laser light source is superior to traditional white light sources that base on blackbody radiation. Supercontinuum light possesses the high intensity and directionality of lasers, and it can be more coherent than a conventional, chaotic white light source.

In the field of spectroscopy, the broad spectrum of SC light allows for many different excitations to be studied using a single light source, and its high intensity results in high sensitivity measurements. The short duration of SC pulses also yield high resolution measurements [13]. Similarly, the benefits of SC light can be exploited for microscopy [14, 15], optical communication [16, 17], and biomedical imaging such as optical coherence tomography (OCT) [18]. Supercontinuum light can also be used as frequency combs, that are precise references for frequency and can be used in, for example, optical clocks [13].

For different applications, it is important to consider the coherence of the SC light. As some of the processes behind SC generation are noise-seeded, light loses its coher-

ence, and thus, supercontinuum cannot be used for certain applications. For example, with applications in metrology and optical communications there is a demand for high coherence, whereas imaging applications may allow the use of less coherent light, or even require light with low-coherence. The measurement of coherence of a SC light source is essential and it is the objective of the experimental work prepared in this thesis.

3 TWO-PHOTON ABSORPTION

Two-photon absorption (TPA) is a phenomenon where two photons are absorbed simultaneously by an atom or a molecule. This is a nonlinear process that becomes relevant when the optical intensity of light is high and thus the probability of two-photon absorption increases [19]. TPA has multiple applications in the field of laser optics due to its nonlinear nature. These applications include for example fluorescence microscopy [20, 21, 22], three-dimensional optical storage memory [23, 24] and autocorrelators [25, 26].

3.1 Basic principle

Two-photon absorption is the simplest form of multiphoton absorption. In single-photon absorption photons can be absorbed if their photon energy is as large as the energy gap between the molecular ground state and one excited state. In multiphoton absorption, however, two or more photons are absorbed simultaneously, if their photon energies combined equal the energy gap such that absorption may occur for photons with a smaller photon energy. In the case of two-photon absorption this means that for a molecule with an energy gap ΔE, two-photon absorption may occur for photons with energy $\Delta E/2$, as two photons are absorbed simultaneously. [27]

The basic principle of two-photon absorption as opposed to single-photon absorption is shown in Figure 3.1. The excitation from the ground state to the excited state in two-photon absorption can be described to take place via a virtual state in-between. TPA can then be considered as two single photons being absorbed successively. This requires that the time difference between the two photons equals or is less than Δt, which is the lifetime of the virtual state determined by the uncertainty principle. The value of Δt is on the order of a fraction of a femtosecond for typical wavelengths used in two-photon excitation, which is less than the oscillation period of such light [27]. This indicates that for TPA to occur, the two photons must interact with the molecule simultaneously.

The transition rate $R^{(1)}$ for single-photon absorption is proportional to the light intensity I

$$R^{(1)} = \sigma^{(1)}(\omega)I, \tag{3.1}$$

where $\sigma^{(1)}$ is the single-absorption cross section, that depends on the frequency ω of the incident light. In contrast, the transition rate $R^{(2)}$ for two-photon absorption is proportional

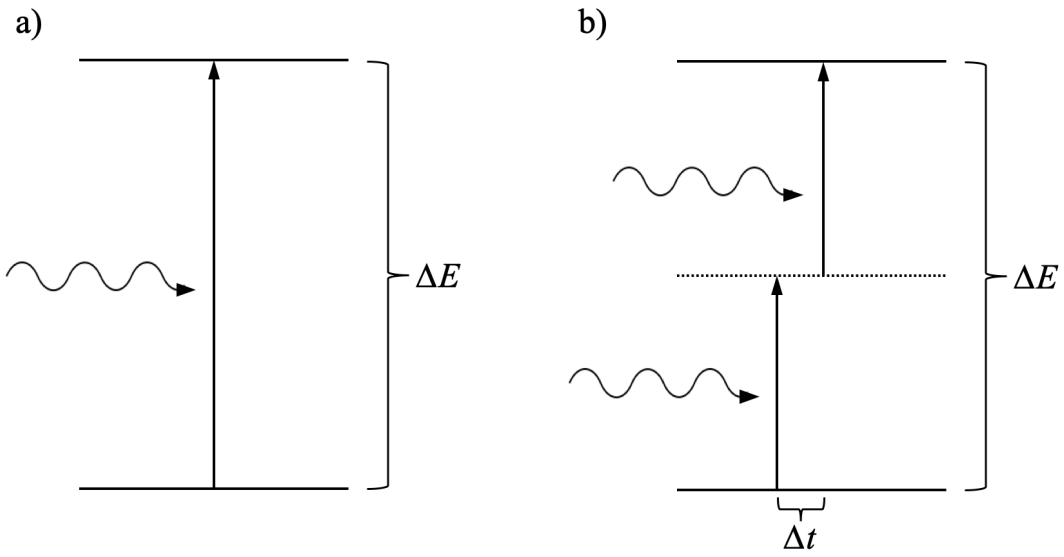

Figure 3.1. *a) Single-photon absorption, where a photon with energy that equals the energy gap ΔE between molecular ground state and excited state is absorbed. b) Two-photon absorption, where the energy gap ΔE is twice as large as the energy of single incident photons, and absorption occurs via a virtual state, represented with a dashed line. The time difference between the photons must be equal to or shorter than Δt. [27]*

to the square of the incident light intensity as

$$R^{(2)} = \sigma^{(2)}(\omega) I^2, \tag{3.2}$$

where $\sigma^{(2)}$ is the two-photon absorption cross section [9]. This quadratic relation between the absorption rate and the optical intensity makes TPA a nonlinear process. For high optical intensities, two-photon absorption dominates over linear absorption, which can be advantageously utilized for applications involving intensity-dependent optical processes [27].

3.2 Applications

The characteristics of two-photon absorption, such as the nonlinear nature, make it suitable for many applications that exploit high intensity lasers. For example, in fluorescence microscopy TPA has enabled significant improvements in three-dimensional scanning resolution. In this technique of microscopy, light is focused to excite a sample at a certain location, causing fluorescence emission, which is detected to obtain an image. A three-dimensional fluorescence microscopy measurement is carried out by using a lens to achieve confocal excitation, which is where two-photon absorption offers an advantage [27].

A three-dimensional measurement based on TPA has a higher resolution than a method based on single-photon absorption because the fluorescence emission scales quadrat-

ically with light intensity when using TPA, compared to scaling linearly, as happens in the case of single-photon absorption [20]. Thus, fluorescence is detected more precisely at the depth wanted, without having additional fluorescence emission above and below the focal plane. Fluorescence microscopy is mostly used in biomedical science to obtain three-dimensional images of organic structures such as cells [21] as well as imaging inorganic materials [22].

TPA can also be utilized in three-dimensional optical storage devices to achieve high capacity [23, 24]. Similarly to fluorescence microscopy, this is because the incident light can be focused to a small spot in the three-dimensional storage medium and, due to the nonlinear response of TPA, information can be precisely written to and read from the focus. Thus, more information can be stored in a medium of a certain volume than would be possible using a method based on single-photon absorption. [23]

Alongside applications on three-dimensional systems, TPA has also been widely used in autocorrelation measurements of ultrashort pulses [25, 26]. In these measurements TPA is typically used instead of second-harmonic generation (SHG) to achieve a nonlinear response. The response can be easily detected with a semiconductor photodiode, making this method cheaper and more convenient than the SHG alternative. Another benefit for using TPA instead of SHG is that TPA does not require fulfilling the phase-matching condition. Commercial devices for TPA detection are available for a wide range of wavelengths, allowing the convenient use of TPA in autocorrelation measurements to characterize ultrashort pulses [28].

4 AUTOCORRELATION MEASUREMENTS

Autocorrelation is a standard technique to characterize ultrashort laser pulses. The terms ultrashort or ultrafast are generally associated with optical pulses that have a duration of picosecond (10^{-12} s) timescale or less. The difficulty in characterizing such short pulses lies in the way that temporal events are traditionally measured using shorter events in time as a reference, which proves difficult with ultrashort pulses, as there are practically no such events available. A way to circumvent this problem is to use the pulse itself as a reference, which is called an autocorrelation measurement. [5]

The basis of autocorrelation measurements is that an input pulse is splitted into two replicas and a variable delay τ is introduced between the two pulses. When delay is varied, the correlation between the two pulses can be measured. Depending on the measurement setup used, the correlation function provides information on the pulses, and in particular an estimate of the pulse duration. [5] However, because the autocorrelation functions are always symmetrical with respect to the center (where $\tau = 0$), the complete intensity and phase information of an optical pulse cannot be resolved with autocorrelation measurements, as the same correlation function can be achieved from different pulse shapes [29].

4.1 Intensity autocorrelation

In order to obtain useful information on pulses using autocorrelation measurements, a simple measurement using a Michelson interferometer and a slow, time-avergaging detector to measure the average power of the interference of pulses as a function of delay is not sufficient. The information acquired this way could easily be reached by measuring the time-averaged power spectrum of the pulses and performing a Fourier transform. Instead, more useful measurements can be done by introducing a nonlinear element to the measurement setup. [5]

A general way to generate a nonlinear response is to use second-harmonic generation (SHG). SHG is a phenomenon, where light with frequency ω propagates through a nonlinear medium, typically an SHG crystal, and generates light with frequency 2ω, which has an intensity quadratical to the incident light intensity [30]. SHG crystals are widely used as a means of generating second-order nonlinearity in autocorrelation measurements [31, 32, 33]. Other means for nonlinear measurements do exist, one of them being

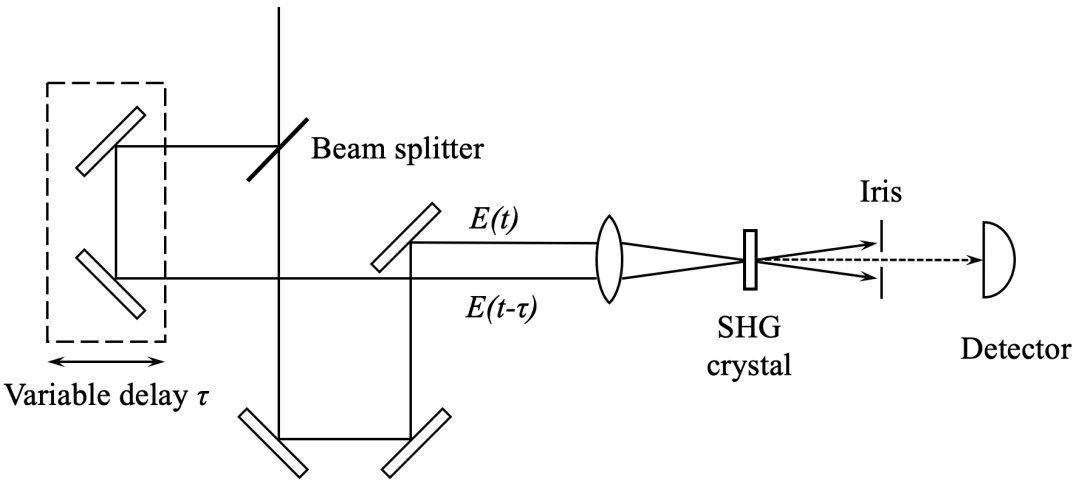

Figure 4.1. *Typical experimental setup for intensity autocorrelation measurement. An incident beam is splitted into two with a beamsplitter, and a variable delay is introduced to one of the beams. The beams overlap in an SHG crystal, inducing an SHG signal that is measured with a detector. An iris prevents the two individual pulses from reaching the detector, making the measurement background-free.*

two-photon absorption (TPA), which is more convenient and cheaper than SHG and it is indeed used widely in autocorrelation measurements [25, 26].

An example of a noncollinear experimental setup for measuring the SHG intensity autocorrelation is illustrated in Figure 4.1. The intensity of the SHG signal is the squared sum of the two electric fields with relative delay τ, and it can be written as

$$[E(t) + E(t-\tau)]^2 = E(t)^2 + E(t-\tau)^2 + 2E(t)E(t-\tau). \tag{4.1}$$

Here the first two terms denote the fields associated with the two delayed pulses, the power of which remains constant as the delay is varied. This is because the detector is slow and the detected signal is averaged over a time-window much longer than the delay between the pulses. In a noncollinear measurement such as is presented in Figure 4.1, the direction of the individual beams differ from that of the SHG signal so they can be eliminated with an iris, leaving only the SHG term to be measured by the detector and making the measurement background-free. The SHG signal varies as the delay is varied, and measuring it over a delay range exceeding the pulse duration yields the intensity autocorrelation (AC) as

$$I_{sig}(\tau) \propto \int_{-\infty}^{\infty} |E^*(t)E(t-\tau)|^2 \, dt = \int_{-\infty}^{\infty} I(t)I(t-\tau)dt, \tag{4.2}$$

where $E^*(t)$ is the complex conjugate of $E(t)$ [5].

The normalized intensity autocorrelation is known as the $G_2(\tau)$ function, which has the form

$$G_2(\tau) = \frac{\langle I(t)I(t-\tau)\rangle}{\langle |I(t)|^2\rangle}, \tag{4.3}$$

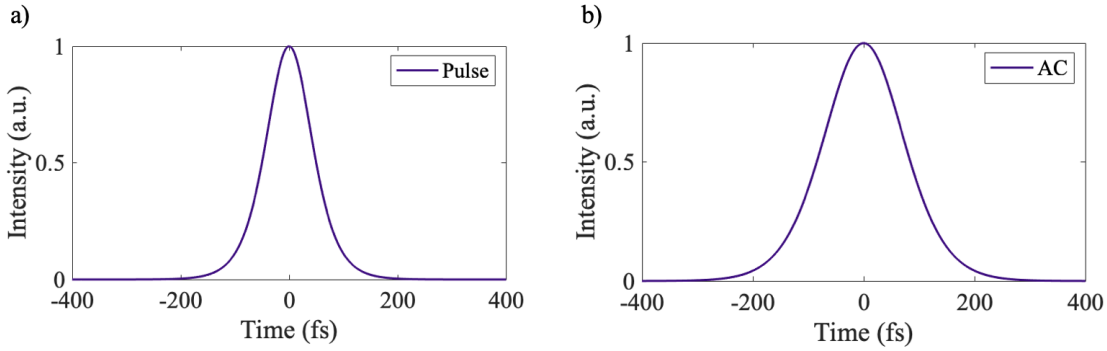

Figure 4.2. *a) A 100-fs sech^2 pulse and b) its intensity autocorrelation.*

where angle brackets denote time-averaging [5]. Examples of normalized intensity autocorrelation functions ($G_2(\tau)$ functions) for theoretical laser pulses are shown in Figure 4.2. The maximum of the autocorrelation function is always at $\tau = 0$ and the trace is always symmetrical with respect to the zero delay, even if the pulse intensity is not. Due to this symmetry, the complete pulse intensity profile cannot be resolved from an AC function, as the same AC function may correspond to multiple pulse shapes.

However, AC measurements are useful for determining the duration of ultrashort pulses. There is a known ratio, a deconvolution factor, between the full width at half maximum (FWHM) value of the AC function and the FWHM of ideal pulse shapes such as a sech or Gaussian [5]. Thus, by calculating the FWHM of the measured AC function and assuming a given pulse shape, an estimate of the FWHM of the pulses can be obtained.

4.2 Interferometric autocorrelation

An autocorrelation measurement, where a collinear setup is used and the signal is measured as a function of delay, yields the interferometric autocorrelation (IAC) trace. Such measurement setup is shown in Figure 4.3. An interferometric autocorrelation trace provides information on the phase and coherence of the incident pulses. One can also infer the conventional intensity autocorrelation function from a simple low-pass filtering procedure. [5]

The interferometric autocorrelation function includes all the terms in Equation 4.1, such that the measured intensity of the SHG signal as a function of τ is now given by

$$I_{sig}(\tau) = \int_{-\infty}^{\infty} \left| E(t)^2 + E(t-\tau)^2 + 2E(t)E(t-\tau) \right|^2 dt. \tag{4.4}$$

By expanding this expression, four terms can be distinguished and the intensity can be

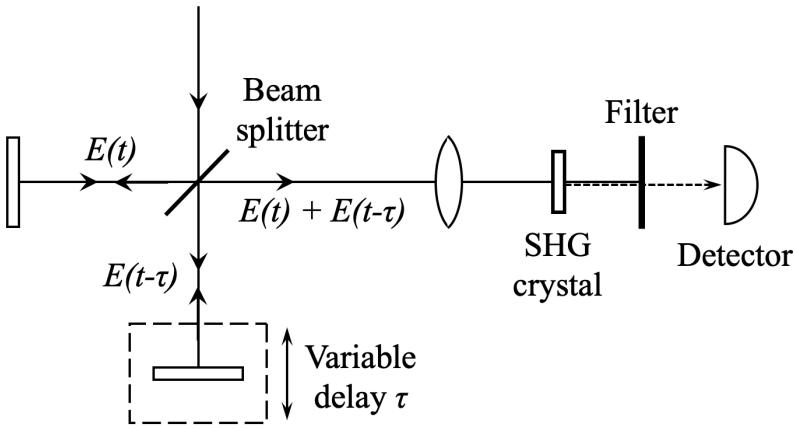

Figure 4.3. *Typical experimental setup for an interferometric autocorrelation measurement. The second harmonic of the two replica of the same pulse reach the detector and interfere with each other.*

written as

$$I_{sig}(\tau) = 2\int_{-\infty}^{\infty} I(t)^2 dt + 4\int_{-\infty}^{\infty} I(t)I(t-\tau)dt + 4\int_{-\infty}^{\infty} I(t-\tau)^2]\Re[E(t)E^*(t-\tau)]dt + 2\int_{-\infty}^{\infty} \Re[E(t)^2 E^*(t-\tau)^2 dt]. \quad (4.5)$$

Here the first term denotes the background signal, independent of τ, caused by the two individual pulses. The second term represents the intensity autocorrelation, while the third and fourth terms represent the interferometric contributions that cause rapid oscillations when τ is varied. The fringes of the third term, the modified interferogram of $E(t)$, occur at a frequency ω and the fringes of the fourth term, the interferogram of the second harmonic of $E(t)$, have a frequency of 2ω [5].

An example of short pulse and its interferometric autocorrelation trace are shown in Figure 4.4. As can be seen from the figure, a ratio of 8:1 should be observed between the peak of the upper envelope of the fringes and the background signal. This ratio can be used to indicate whether an IAC measurement is valid. The lower side of the envelope approaches zero near τ = 0 due to destructive interference. [5]

As previously mentioned, the IAC function contains the intensity autocorrelation (AC) term. The AC function can be retrieved from an IAC trace by low-pass filtering out the rapidly oscillating terms, ie. the third and fourth term of Equation 4.5. The low-pass filtering can be done by using a Fourier transform, filtering high frequencies, and performing an inverse Fourier transform to return to the time domain. After low-pass filtering, a ratio of 3:1 between the peak and the background term should be observed. After substracting the constant background (ie. 1 for an AC of pulsed light) from a low-pass filtered trace that has been normalized relative to the background signal, the AC function will have a maximum value of 2 at τ = 0, and it will decay to 0 as delay increases [5].

An interferometric autocorrelation trace also contains some information on the coherence

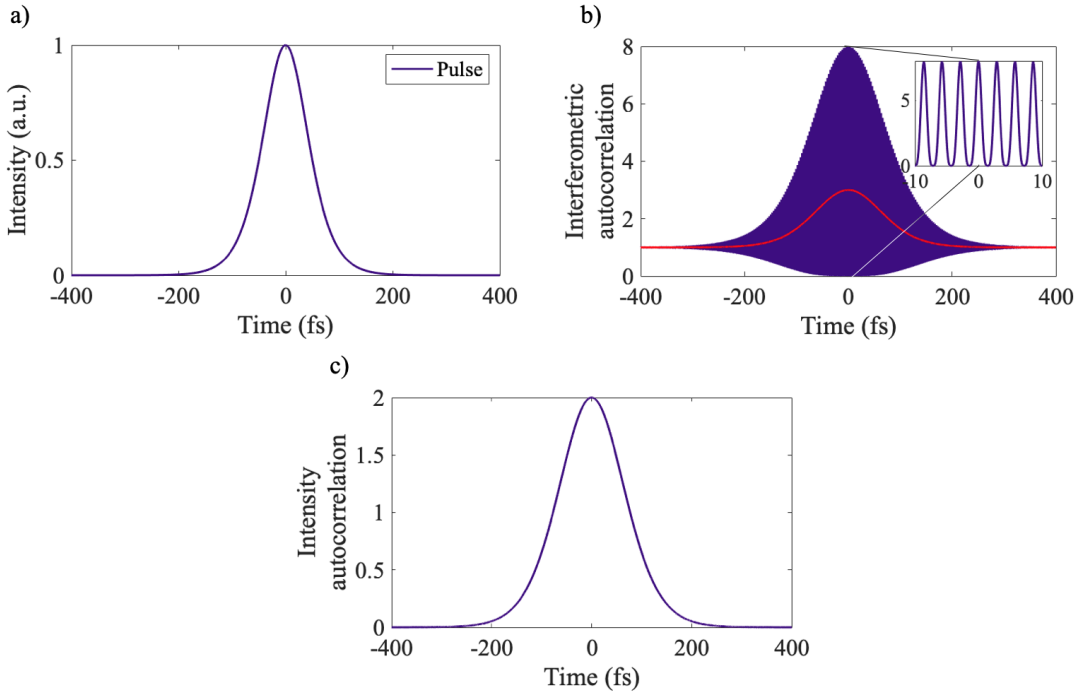

Figure 4.4. *a) A 100-fs sech^2 pulse and b) its interferometric autocorrelation. The interferogram consists of rapid oscillations caused by the interference of two pulse replicas. An intensity autocorrelation, (coloured red) can be retrieved from the interferometric autocorrelation trace by filtering out the fast oscillating components. After substracting background intensity, a conventional intensity autocorrelation trace is obtained as shown in c).*

and phase stability of the measured pulses. The time interval over which interference (oscillation) is observed in an IAC trace is related to the coherence time τ_c of the light. The longer the coherence time is, the more coherent the light is. The phase stability information acquired with an interferometric autocorrelation measurement is essentially qualitative, indicated by whether modulation is present or not as well as the modulation depth. The presence of phase modulation causes a narrower interference pattern to the interferometric autocorrelation. An IAC trace can also be used to quantitatively measure linear chirp of pulses, even though the presence of chirp could also be deduced from the time-bandwidth product of the pulses. A measure of the chirp in the IAC trace is the level at which the interference begins relative to the peak [29].

5 EXPERIMENTS

This chapter introduces the experiments on measuring the interferometric autocorrelation of supercontinuum light using TPA. The experiments were carried out in the Photonics laboratory at the Tampere University in the Ultrafast Optics research group.

5.1 Setup

An illustration of the laboratory setup used in the experiments is shown in figure 5.1. Laser pulses are generated by a Ti:Sapphire laser (Spectra-Physics Tsunami) with a tunable wavelength set to 860 nm, a duration of 210 fs, and a repetition rate of 80 MHz. The supercontinuum is generated in the regime of anomalous dispersion by injecting the laser pulses into a photonic crystal fiber (PCF, Thorlabs NL-2.8-850-02) with a zero-dispersion wavelength (ZDW) of 850 nm, a dispersion slope of 0.48 ps/nm^2/km and a nonlinear coefficient of 47 W^{-1}km^{-1}.

The generated supercontinuum pulses are directed to a Michelson interferometer, which consists of two mirrors and a beam splitter dividing the light into two identical pulse trains. One of the interferometer mirrors is fixed and the other is placed on a stage that is moved with a piezoelectric motor (SmarAct SLC-2430) to control the relative delay of the pulses with up to 4 nm precision.

After the interferometer the light is focused with an aspheric lens to a GaP photodetector operating over the wavelength range of 150-550 nm. A long-pass filter is used to ensure that shorter wavelengths of the supercontinuum do not reach the detector. This is to avoid direct single-photon absorption at the detector, but to allow two-photon absorption to be detected for wavelengths ranging from 550 nm to 1100 nm, which covers the range of the supercontinuum. Finally, an oscilloscope is used to record the signal from the photodetector. The measurement system is controlled with a LabVIEW program.

Due to inpurities in the detector material, some residual, linear absorption occurs for wavelengths outside the photodetector range. This linear absorption is the main difficulty in measuring the interferometric autocorrelation of supercontinuum light with two-photon absorption method, as the linear contribution may dominate over TPA for weaker spectral components of the SC.

The linear contribution can be eliminated by tuning the nonlinear response of two-photon

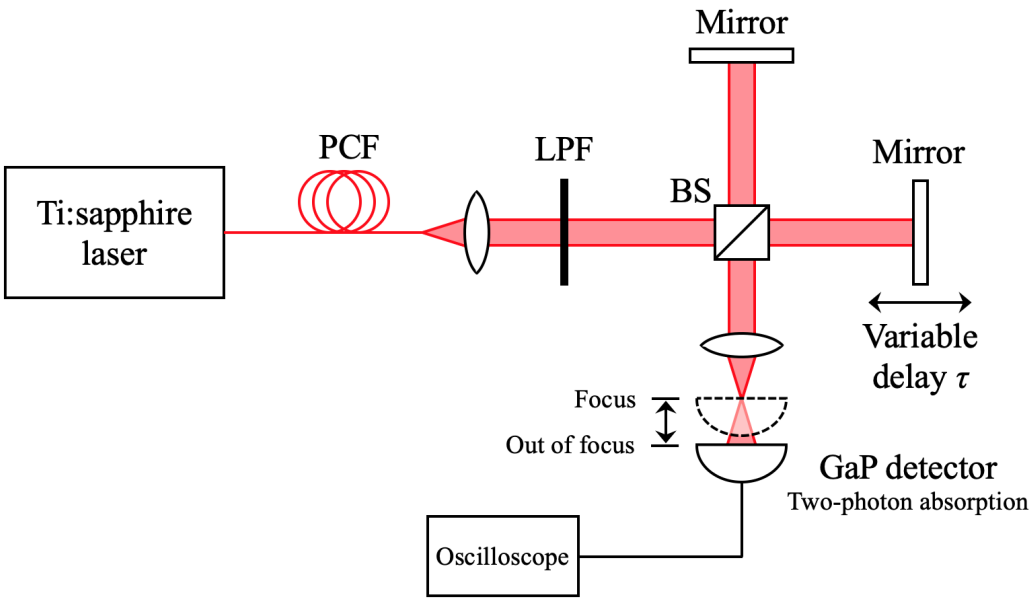

Figure 5.1. *Experimental setup used for the IAC measurements of SC light. A Photonic Crystal Fiber (PCF) is used to generate a supercontinuum from short laser pulses. Light is guided to a Michelson interferometer and splitted into two with a beam splitter (BS). A variable delay is introduced into one arm of the interferometer. An aspheric lens is used to focus light to a GaP photodetector, which is connected to an oscilloscope to measure the IAC signal. A low-pass filter (LPF) is inserted to prevent linear absorption in the detector.*

absorption. If the detector is moved out of the focal plane of the lense focusing the light, the intensity of light at the detector is substantially decreased, making TPA practically non-existent. This way, the mere linear absorption can be measured, and it can be substracted from the signal measured at the focal plane of the lense, allowing access to the pure two-photon absorption signal.

5.2 Results

Interferometric autocorrelation measurements with the setup described above were carried out using different input peak powers to generate supercontinuum light. The results concentrate on generating the SC with relatively low input peak power (coherent supercontinuum) and high input peak power (incoherent supercontinuum). The spectra of the generated supercontinua are measured with an Optical Spectrum Analyzer (OSA). The obtained IAC results are discussed and observations are made on the coherence properties.

It should be noted that the measurements were taken for delay points corresponding to only half of the interferogram starting from the zero delay position. The data were mirrored after the measurement to obtain the full interferogram. This was done in order to save measurement time, as the fiber coupling might not be stable for extended periods of time. The mirroring is justified because, as explained in Chapter 4, an IAC trace is symmetrical

according to the zero delay axis when the interferometer is properly aligned.

5.2.1 Coherent supercontinuum

The spectrum of the supercontinuum generated with relatively low input peak power ($P_p \approx$ 420 W) spans roughly from 750 nm to 950 nm and is shown in Figure 5.2a. The measured interferograms for the data measured at the focus and out-of-focus plane are shown in Figure 5.2b. The temporal resolution of the measurement is approximately 0.27 fs, as the interferometer mirror is moved in steps of 40 nm.

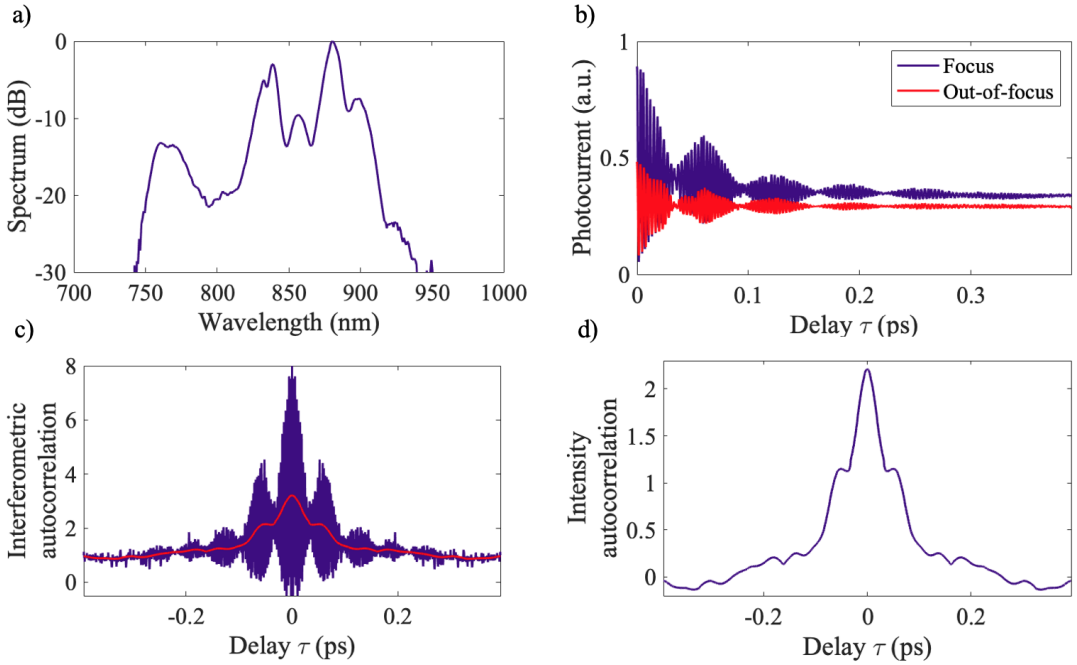

Figure 5.2. *Results for coherent supercontinuum. a) Spectrum measured with the OSA. b) Measured interferogram in the focus plane and out-of-focus plane of the lens. c) Interferometric autocorrelation trace obtained by mirroring the measured data. The red line represents the low-pass filtered trace. d) Intensity autocorrelation function extracted from the interferometric autocorrelation trace.*

The interferometric autocorrelation trace (Figure 5.2c) is obtained by substracting the focus and out-of-focus data from each other as described previously. The IAC trace indicates a 8:1 ratio between the peak and the background signal, indicating a successful measurement. Oscillation are observed across the full trace and the coherence time is approximately 300 fs, meaning that the light appears to be essentially coherent. The trace has multiple side-lobes with fast oscillations, which indicate that the coherent supercontinuum pulses have phase-stable sub-structures in the temporal domain.

The intensity autocorrelation extracted from the IAC trace by low-pass filtering and substracting the background signal is shown in Figure 5.2d. The peak of the AC function is around 2 and the tail draws near 0 as expected for pulsed light.

5.2.2 Incoherent supercontinuum

With increased input peak power, P_p = 18 kW, the generated supercontinuum spans from 550 nm to 1300 nm, as seen in Figure 5.3a. After the long-pass filter, the wavelengths shorter than 750 nm are filtered out to prevent linear absorption, as the detector detects wavelengths up to 700 nm and slightly above. Also, the detector only detects wavelengths until 1100 nm, so longer wavelengths than 1100 nm are also filtered out.

The measured interferogram for this supercontinuum is shown in Figure 5.3b. This measurement was done in two parts to reduce the overall measurement time and also minimize the possible thermal effects during the measurement. The oscillating center part was measured with smaller step size (30 nm), whereas the long tail was measured with increased step size (1.5 μm) and iterpolated.

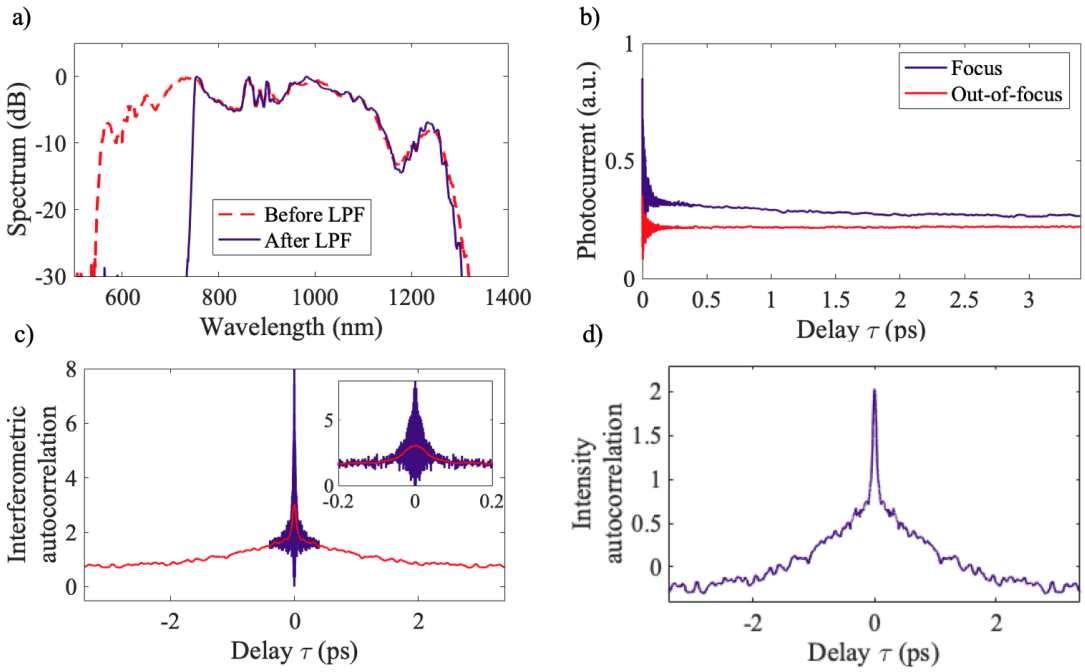

Figure 5.3. *Results for incoherent supercontinuum. a) Spectrum measured with the OSA before and after a long-pass filter (LPF). b) Measured interferogram in the focus plane and out-of-focus plane of the lens. c) Interferometric autocorrelation trace obtained by mirroring the measured data. The red line represents the low-pass filtered trace. The oscillation occurs only on the very center part of the trace. d) Intensity autocorrelation function extracted from the interferometric autocorrelation trace.*

Figure 5.3c shows the resulting interferometric autocorrelation trace, which has a clear peak-to-background ratio of 8:1. Here the oscillations occur only in the central part and no side-lobes are visible. The coherence time is approximately 75 fs, much shorter than when using lower input peak power, indicating that the supercontinuum light generated with higher peak power has a more incoherent nature. Around the fast oscillating center part, the peak-to-background ratio is 8:2, which is typical for a chaotic light source [34].

The intensity autocorrelation retrieved from the IAC trace by low-pass filtering out the

high frequencies is shown in Figure 5.3d. The width of the central peak gives an estimate of 120 fs as the average duration of the sub-pulses present under the broader temporal envelope. The witdh of the whole AC trace reveals the entire duration of the SC pulses, which is nearly 4 ps. When concentrating on the central spike only, the ratio from the peak to the edges is close to 2:1, which is typical for chaotic light [5].

6 CONCLUSION

This thesis presented interferometric autocorrelation measurements of supercontinuum light. The measurement method is based on two-photon absorption, which makes the measurement cheaper and more convenient than other available interferometric autocorrelation techniques. The characterization of supercontinuum light is important as many applications require specific coherence properties.

The supercontinuum was generated in the regime of anomalous dispersion of a photonic crystal fiber, which results into a broad spectrum. The interferometric autocorrelation trace is captured by using a semiconductor GaP photodetector to measure two-photon absorption, a nonlinear process that can be conveniently used for autocorrelation measurements. Due to inpurities in the GaP detector, some residual linear absorption occurs in the measurement, but this linear absorption can be eliminated by performing measurements both in and out the focus of the lens that focuses light onto the detector.

The IAC measurements were performed for coherent and incoherent SC. In the case of coherent SC, the input peak power is relatively low, and the obtained interferometric autocorrelation trace exhibits interference over the entire trace with a corresponding coherence time of 300 fs. For incoherent SC, the input peak power is higher, and the coherence occurs over only 75 fs. In addition to the quantitative coherence information, the envelope of the IAC trace also reveals that the coherent SC light generated with lower peak power has side lobes, indicating phase-stable sub-pulses in the temporal domain, whereas for incoherent SC they are not visible.

Based on the discussed results, it is confirmed that the second-order coherence properties of SC light can be tuned by varying the input peak power. Thus, the coherence properties can be tailored for specific applications. The measurement technique proves to be simple and efficient for inspecting the coherence properties of supercontinuum light, which is beneficial for further use and research.

REFERENCES

[1] R. Alfano and S. Shapiro. Emission in the region 4000 to 7000 via four-photon coupling in glass. *Physical Review Letters* 24.11 (1970).

[2] X. Gu, M. Kimmel, A. Shreenath, R. Trebino, J. Dudley, S. Coen and R. Windeler. Experimental studies of the coherence of microstructure-fiber supercontinuum. *Optics express* 11.21 (2003).

[3] X. Gu, L. Xu, M. Kimmel, E. Zeek, P. O'Shea, A. P. Shreenath, R. Trebino and R. S. Windeler. Frequency-resolved optical gating and single-shot spectral measurements reveal fine structure in microstructure-fiber continuum. *Optics letters* 27.13 (2002).

[4] G. Genty, M. Surakka, J. Turunen and A. T. Friberg. Complete characterization of supercontinuum coherence. *Optics letters* 28.9 (2011).

[5] A. M. Weiner. *Ultrafast Optics*. 2009.

[6] J. M. Dudley, G. Genty and S. Coen. Supercontinuum generation in photonic crystal fiber. *Reviews of Modern Physics* 78.4 (2006).

[7] G. P. Agrawal. *Nonlinear Fiber Optics*. 4th ed. 2007.

[8] E. Hecht. *Optics*. 5th ed. 2017.

[9] R. W. Boyd. *Nonlinear optics*. 3rd ed. 2008.

[10] S. B. Cavalcanti and G. P. Agrawal. Noise Amplification in Dispersive Nonlinear Media. *Physical review. A, Atomic, molecular, and optical physic* 51.5 (1995).

[11] S. Coen, A. H. L. Chau, R. Leonhardt, J. D. Harvey, J. C. Knight, W. J. Wadsworth and P. S. J. Russell. Supercontinuum Generation by Stimulated Raman Scattering and Parametric Four-Wave Mixing in Photonic Crystal Fibers. *Journal of the Optical Society of America B* 19.4 (2004).

[12] R. A. Sergeevič and N. O. Evgenévič. *Wikimedia Commons - File:Photonic-crystal fiber.jpg*. Licensed under CC BY-SA 3.0 (https://creativecommons.org/licenses/by-sa/3.0/deed.en). URL: `https://commons.wikimedia.org/wiki/File:Photonic-crystal_fiber.jpg` (visited on 06/28/2020).

[13] P. Hannaford. *Femtosecond Laser Spectroscopy*. 2005.

[14] S. Dupont, C. Petersen, J. Thøgersen, C. Agger, O. Bang and S. R. Keiding. IR Microscopy Utilizing Intense Supercontinuum Light Source. *Optics express* 20.5 (2012).

[15] Y. Liu, H. Tu, W. A. Benalcazar, E. J. Chaney and S. A. Boppart. Multimodal Nonlinear Microscopy by Shaping a Fiber Supercontinuum From 900 to 1160 nm. *IEEE Journal of Selected Topics in Quantum Electronics* 18.3 (2012).

[16] Z. Sun, T. Wang, Z. Jiang, P. Lin, J. Chen, X. Zhang, P. Chen and Y. Zhao. A High SNR Partially Coherent Beam Source Based on Supercontinuum for Free Space Data Transmission. *Optics Communications* 450 (2019).

[17] T. Ohara, H. Takara, T. Yamamoto, H. Masuda, T. Morioka, M. Abe and H. Takahashi. Over-1000-Channel Ultradense WDM Transmission with Supercontinuum Multicarrier Source. *Journal of Lightwave Technology* 24.6 (2006).

[18] J. Barrick, A. Doblas, M. R. Gardner, P. R. Sears, L. E. Ostrowski and A. L. Oldenburg. High-speed and high-sensitivity parallel spectral-domain optical coherence tomography using a supercontinuum light source. *Optics Letters* 41.24 (2016).

[19] N. V. Tkachenko. *Optical spectroscopy: methods and instrumentations*. 1st ed. 2006, Appendix C.

[20] W. Denk, J. H. Strickler and W. W. Webb. Two-Photon Laser Scanning Fluorescence Microscopy. *Science* 248.4951 (1990).

[21] V. P. Tokar, M. Y. Losytskyy, T. Y. Ohulchanskyy, D. V. Kryvorotenko, V. B. Kovalska, A. O. Balanda, I. M. Dmytruk, V. M. Prokopets, S. M. Yarmoluk and V. M. Yashchuk. Styryl Dyes as Two-Photon Excited Fluorescent Probes for DNA Detection and Two-Photon Laser Scanning Fluorescence Microscopy of Living Cells. *Journal of Fluorescence* 20.4 (2010).

[22] A. Al-Tabich, W. Inami, Y. Kawata, R. Jablonski, S. Worasawat and H. Mimura. 3D imaging of intrinsic crystalline defects in zinc oxide by spectrally resolved two-photon fluorescence microscopy. *Applied Physics Letters* 110.22 (2017).

[23] A. Dvornikov, E. Walker and P. Rentzepis. Two-photon three-dimensional optical storage memory. *Journal of Physical Chemistry A* 113.49 (2009).

[24] J. Cai and W. Huang. Two-photon three-dimensional optical storage of a new pyrimidine photobleaching material. *Optik - International Journal for Light and Electron Optics* 126.3 (2015).

[25] F. Laughton, J. Marsh, D. Barrow and E. Portnoi. The two-photon absorption semiconductor waveguide autocorrelator. *IEEE Journal of Quantum Electronics* 30.3 (1994).

[26] K. Kondo and T. Baba. High-performance on-chip autocorrelator using a rib waveguide loaded with two-photon absorption diodes. *Optics Letters* 43.4 (2018).

[27] D. L. Andrews. *Fundamentals of photonics and physics*. 2015.

[28] D. Reid, W. Sibbett, J. Dudley, L. Barry, B. Thomsen and J. Harvey. Commercial Semiconductor Devices for Two Photon Absorption Autocorrelation of Ultrashort Light Pulses. *Optics Letters* 37.34 (1998).

[29] J.-C. Diels and W. Rudolph. *Ultrashort laser pulse phenomena: fundamentals, techniques, and applications on a femtosecond time scale*. 2006.

[30] F. Träger. *Springer Handbook of Lasers and Optics*. 2012.

[31] K. Naganuma, K. Mogi and H. Yamada. Time direction determination of asymmetric ultrashort optical pulses from second-harmonic generation autocorrelation signals. *Applied Physics Letters* 54.13 (1989).

[32] J. Paye. How to Measure the Amplitude and Phase of an Ultrashort Light Pulse with an Autocorrelator and a Spectrometer. *IEEE Journal of Quantum Electronics* 30.11 (1994).

[33] R. Panda and S. K. Das. Fringe resolved autocorrelator for characterization of ultrashort laser pulses using second harmonics of ZnO nanorods. *Optics Communications* 11.402 (2017).

[34] S. Toenger, R. Mäkitalo, J. Ahvenjärvi, P. Ryczkowski, M. Närhi, J. M. Dudley and G. Genty. Interferometric Autocorrelation Measurements of Supercontinuum based on Two-Photon Absorption. *Journal of the Optical Society of America B* 36.5 (2019).